Liquid-vapor interface of a polydisperse fluid

Matteo Buzzacchi and Nigel B. Wilding

Department of Physics, University of Bath, Bath BA2 7AY, United Kingdom

(Received 25 February 2005; published 28 June 2005)

We report a grand canonical Monte Carlo simulation study of the liquid-vapor interface of a model fluid exhibiting polydispersity in terms of the particle size σ. The bulk density distribution, $\rho^0(\sigma)$, of the system is controlled by the imposed chemical potential distribution $\mu(\sigma)$, the form of which is specified such that $\rho^0(\sigma)$ assumes a Schulz form with associated degree of polydispersity $\approx 14\%$. By introducing a smooth attractive wall, a planar liquid-vapor interface is formed for bulk state points within the region of liquid-vapor coexistence. Owing to fractionation, the pure liquid phase is enriched in large particles, with respect to the coexisting vapor. We investigate how the spatial variation of the density near the liquid-vapor interface affects the evolution of the local distribution of particle sizes between the limiting pure phase forms. We find [as previously predicted by density-functional theory, Bellier-Castella *et al.*, Phys. Rev. E **65**, 021503 (2002)] a segregation of smaller particles to the interface. The magnitude of this effect as a function of σ is quantified via measurements of the relative adsorption. Additionally, we consider the utility of various estimators for the interfacial width and highlight the difficulty of isolating the intrinsic contribution of polydispersity to this width.

I. INTRODUCTION AND BACKGROUND

Complex fluids in which the particles are similar in character but not strictly identical are termed polydisperse. Examples arise throughout soft matter science, notably in colloidal dispersions, polymer solutions, and liquid crystals. Typically the polydispersity of such systems is manifest as a variation in some physical attribute such as particle size, shape, or charge, which is customarily denoted by a continuous parameter σ. The form of the polydispersity is then quantifiable in terms of a distribution $\rho(\sigma)$ measuring the number density of particles of each σ. Consequently, one can regard the system as a mixture of an infinite number of particle "species" each labeled by the value of σ [1].

As has long been appreciated, polydispersity can profoundly influence the thermodynamical and processing properties of complex fluids [2–5], making a clear elucidation of its detailed role a matter of both fundamental and practical importance. The majority of recent effort in this regard has focused on clarifying the bulk phase behavior of polydisperse systems (see [6] for a recent review), which is known to be considerably richer in both variety and character than that of corresponding monodisperse systems. The source of this richness can be traced to *fractionation* effects: at coexistence a polydisperse fluid described by some initial "parent" distribution, $\rho^0(\sigma)$, may divide into two or more "daughter" phases $\rho^{(\alpha)}(\sigma), \alpha=1, 2,\ldots$, each of which differs in composition from the parent. The sole constraint is that the volumetric average of the daughter distributions equals the parent distribution.

The effect of fractionation on phase diagrams can be dramatic. For instance, the familiar liquid-vapor binodal in the density-temperature plane of a monodisperse fluid splits into cloud and shadow curves [6], as shown schematically in Fig. 1(a). These mark, respectively, the density of the onset of phase separation and the density of the incipient (shadow)

phase. The critical point occurs neither at the extremum of the cloud curve nor that of the shadow curve, but at their *intersection*. One implication of this is that even at the critical temperature, liquid vapor coexistence can occur provided the overall parent density is less than its critical value. Additional insight into fractionation effects can be gleaned from the pressure-temperature plane of the phase diagram. In a monodisperse system, coexistence occurs along a line in this plane which terminates at the critical point. However, the introduction of polydispersity broadens this line into a *region*
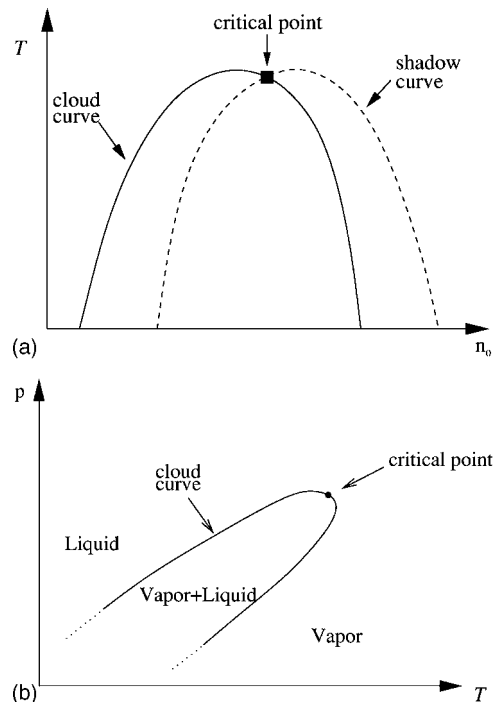

FIG. 1. Schematic phase diagram as described in the text. (a) The density-temperature plane. (b) The pressure-temperature plane.

having a "banana"-like shape [7,8]. The critical point generally lies neither at a point of maximum temperature nor maximum pressure on the perimeter of this region [Fig. 1(b)]. Traversing the coexistence region from one pure phase to the other (e.g., along an isobar or isotherm) corresponds to *smoothly* varying the relative volumes of the system occupied by the two coexisting phases, with concomitant smooth variation in the forms of the daughter distributions.

In view of the richness of the bulk phase behavior, it is natural to enquire how polydispersity influences fluid interfacial properties. Previous work on this subject has largely been limited to the study of size-disperse hard spheres either at a single hard wall [9–12] or confined to a planar slit [13,14]. These investigations focused principally on the effect of the wall on the local fluid structure and distribution of particle sizes. However, since no explicit interparticle attraction was considered, issues of wetting and fluid-fluid coexistence did not arise. The sole previous study of a fluid-fluid interface in a polydisperse system (of which we are aware) is the density-functional theory study of Bellier-Castella *et al.* [15]. Building on previous studies of a homogeneous polydisperse van der Waals fluid [8], these authors obtained the density profiles for various species across a planar liquid-vapor interface. Their calculations indicated a preferential adsorption of small particles at the interface which they reported to be broadened with respect to the monodisperse limit.

In the present work, we have attempted to extend the understanding of interfacial behavior in polydisperse fluids by performing detailed Monte Carlo simulations of a system of spherical size-disperse particles interacting via a Lennard-Jones potential. The simulations are carried out within the grand canonical ensemble and employ a chemical potential distribution $\mu(\sigma)$, the form of which is chosen so as to yield a bulk density distribution $\rho^0(\sigma)$ having a fixed Schulz form, with associated degree of polydispersity $\approx 14\%$. The imposition of such "fixed polydispersity" corresponds to the experimental situation in, for example, colloidal dispersions or polymer solutions, where the form of the parent distribution is prescribed by the synthesis process of the particles, and only its scale can change depending on the quantity of solvent present.

II. METHOD

A. Model and observables

The model we consider comprises a system of particles interacting via an interparticle potential of the Lennard-Jones (LJ) form,

$$u_{ij} = 4\epsilon_{ij}\left[\left(\frac{\sigma_{ij}}{r_{ij}}\right)^{12} - \left(\frac{\sigma_{ij}}{r_{ij}}\right)^6\right]. \quad (2.1)$$

Here $r_{ij} = |\mathbf{r}_i - \mathbf{r}_j|$ is the particle separation and we employ the mixing rules $\sigma_{ij} = (\sigma_i + \sigma_j)/2$ and $\epsilon_{ij} = \epsilon\sigma_i\sigma_j$. A cutoff was applied to the potential for particle separations $r_{ij} > 2.5\sigma_{ij}$.

Conventionally the state of such a fluid in the bulk is described by a parent density distribution $\rho^0(\sigma)$, which can be written [1]
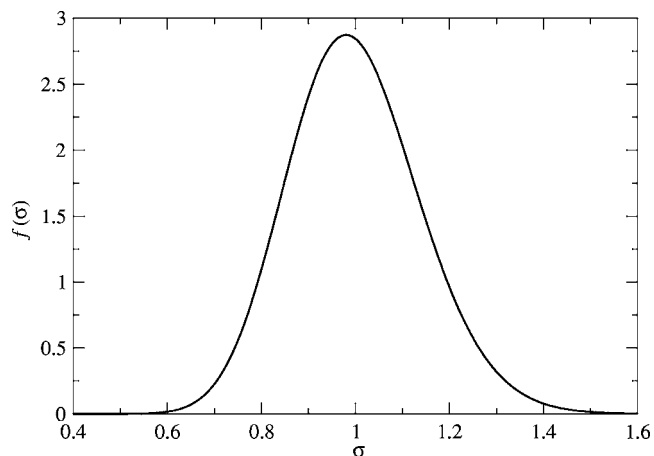

FIG. 2. The Schulz parent size distribution $f(\sigma)$ studied in this work.

$$\rho^0(\sigma) = n_0 f(\sigma). \quad (2.2)$$

Here $n_0 = N/V$ is the overall particle number density, while $f(\sigma)$ is a normalized shape function whose average value $\bar{\sigma}$ serves to set the scale for all lengths. Since the form of $f(\sigma)$ is fixed, the bulk phase diagram is spanned by n_0 and the temperature T [cf. Fig. 1(a)].

A commonly used measure of the scale of variation in the particle diameters is provided by the dimensionless degree of polydispersity, defined as the standard deviation of the parent distribution, normalized by its mean,

$$\delta = \frac{\sqrt{\overline{(\sigma - \bar{\sigma})^2}}}{\bar{\sigma}}. \quad (2.3)$$

In the present work, we have elected to study a parent of the Schulz form,

$$f(\sigma) = \frac{1}{Z!}\left(\frac{Z+1}{\bar{\sigma}}\right)^{Z+1}\sigma^Z\exp\left[-\left(\frac{Z+1}{\bar{\sigma}}\right)\sigma\right]. \quad (2.4)$$

Here the parameter Z controls the width of the distribution and thence the value of δ. We have considered the case $Z = 50$, corresponding to $\delta = (Z+1)^{-1/2} \simeq 0.14$. The resulting form of $f(\sigma)$ is shown in Fig. 2. Note that in contrast to, for example, a Gaussian, the Schulz distribution vanishes smoothly (has a natural cutoff) as $\sigma \rightarrow 0$. For the purposes of the MC simulations described below, however, one does require an upper cutoff in σ, beyond which $f(\sigma)$ is truncated. We set this to be $\sigma_c = 1.6$.

In general, a polydisperse fluid described by Eqs. (2.1) will exhibit liquid-vapor coexistence within the region of the phase diagram enclosed by the cloud curve (cf. Fig. 1). For such coexistence states, a liquid-vapor interface can be formed by introducing a sufficiently attractive wall in the plane $z = 0$. In this work, the particle-wall interactions are assigned the form

$$u_{pw}(\sigma_i, z_i) = \epsilon_w \sigma_i \bar{\sigma} \left[\frac{2}{5} \left(\frac{\sigma_{iw}}{z_i} \right)^{10} - \left(\frac{\sigma_{iw}}{z_i} \right)^4 \right], \qquad (2.5)$$

where $\sigma_{iw} = (\sigma_i + \bar{\sigma})/2$. The form of this potential derives from regarding the wall as a monolayer of monodisperse particles having diameter $\bar{\sigma}$ and interacting with fluid particles via Eq. (2.1).

In order to quantify the resulting interfacial properties, we consider the ensemble averaged local-density distribution $\rho(\sigma, z)$ at a perpendicular distance z from the wall,

$$\rho(\sigma, z) = \int_0^{L_x} \int_0^{L_y} \rho(\sigma, \mathbf{r}) dx dy. \qquad (2.6)$$

We shall also find it useful to define a number of one-dimensional profiles which derive from $\rho(\sigma, z)$. These are the overall density profile,

$$\rho(z) = \int d\sigma \, \rho(\sigma, z); \qquad (2.7)$$

the density profile for a given σ,

$$\rho(z|\sigma) = \int d\sigma' \, \rho(\sigma', z) \delta(\sigma - \sigma'); \qquad (2.8)$$

the volume fraction profile,

$$\eta(z) = \frac{\pi}{6} \int d\sigma \, \rho(\sigma, z) \sigma^3; \qquad (2.9)$$

the local concentration distribution,

$$\phi(\sigma, z) = \frac{\rho(\sigma, z)}{\rho(z)}; \qquad (2.10)$$

and finally [in analogy with Eq. (2.2)], the local normalized size distribution,

$$f(\sigma|z) = \frac{\rho(\sigma|z)}{\int d\sigma \, \rho(\sigma|z)}, \qquad (2.11)$$

with $\rho(\sigma|z) = \int dz' \, \rho(\sigma, z') \delta(z - z')$.

The utility of all these quantities will become apparent in Sec. III.

B. Simulation methodology

The grand canonical Monte Carlo algorithm we have utilized employs four types of operation: particle displacements, deletions, insertions, and resizing. The particle diameter σ is treated as a continuous variable throughout. Observables, on the other hand [principally the form of $\rho(\sigma, z)$], are accumulated as histograms, formed by discretizing into bins the permitted ranges of $\sigma < \sigma_c$ (see Sec. II A) and z (i.e., $0 < z < L_z$). The bin widths used were $\delta\sigma = 0.02$ and $\delta z = 0.02$. Further details of the implementation can be found elsewhere [16].

The algorithm requires as input a chemical potential distribution $\mu(\sigma)$. Given a nominated shape function $f(\sigma)$, specification of the overall density n_0 and the temperature T

serves to fix the bulk form of $\mu(\sigma|n_0, T)$. The assumption that the confined fluid exists in equilibrium with a bulk reservoir implies that both the bulk and confined systems have equal $\mu(\sigma)$. Thus in order to perform simulations of the fluid at a wall, we first require the form of $\mu(\sigma)$ at specified points inside the bulk coexistence region. For the present work, we have focused on the critical isotherm $\widetilde{T}_c = k_B T_c / \epsilon = 1.384$, the critical temperature having been determined in a separate study [17]. Recall (Sec. I) that liquid-vapor coexistence can occur in a polydisperse fluid even at the critical temperature, provided that the overall density n_0 is intermediate between the cloud point and the critical point densities. At $\widetilde{T}_c$, the cloud point occurs at $n_0 = 0.044(1)$ and the critical point at $n_0 = 0.326(2)$.

Using fully periodic simulations, we have determined the form of $\mu(\sigma)$ for a selection of values of n_0 along the critical isotherm between the cloud point and the critical point. For this purpose, the combined techniques of nonequilibrium potential refinement and histogram reweighting were utilized. A description of the procedure has been previously presented in Refs. [18–20] and we again refer the interested reader to these papers for full details.

The resulting forms of $\mu(\sigma|n_0, \widetilde{T}_c)$ for the respective values of n_0 were then used to study the effects of introducing two oppositely facing walls at $z = 0$ and $z = L_z$ (the system remaining periodic in the x and y directions). The system size was set to be $L_x = L_y = 15\bar{\sigma}, L_z = 40\bar{\sigma}$. Interactions between the particles and the wall at $z = 0$ were assigned the form Eq. (2.5), while a simple hard (impenetrable) wall condition was applied at $z = L_z$. This arrangement ensures that only the wall at $z = 0$ can become wet.

For values of n_0 near the cloud point, a moderately thick layer was observed at the wall, extending in the z direction and uniform in the $x-y$ plane. The histogram of the interfacial profile $\rho(\sigma, z)$ presented below corresponds to the choice of parameters $n_0 = 0.089$, $\widetilde{T} = \widetilde{T}_c = 1.384$, with a wall strength $\epsilon_w = 8.3\epsilon$. The resulting liquidlike layer was found to have a thickness of approximately $14\bar{\sigma}$. This is sufficiently large that the liquid-vapor interface can be considered to be essentially decoupled from either wall, a view that was confirmed by comparing the liquid and vapor properties on either side of the interface with those obtained in the corresponding bulk simulations.

In the course of the simulations, the form of $\rho(\sigma, z)$ was observed to exhibit large, slow fluctuations in which the layer thickness varied in the range $12\bar{\sigma}-18\bar{\sigma}$. These fluctuations complicate the task of accumulating high statistics for the intrinsic profile shape because an ensemble average over independent configurations will be considerably smeared out in the z direction. To circumvent this problem we have accumulated a *centered profile* $\rho(\sigma, z^\star)$, whereby the instantaneous profile $\tilde{\rho}(\sigma, z)$ is first shifted with respect to some nominal origin (center) before being accumulated in the histogram. The center of $\tilde{\rho}(\sigma, z)$ was itself determined by measuring the running integral $\int_0^z \tilde{\rho}(\sigma, z') dz'$. This quantity manifests a smoothed discontinuity at the interface center, the location of which can be estimated from the intersection of respective linear fits in the pure vapor and liquid regions well
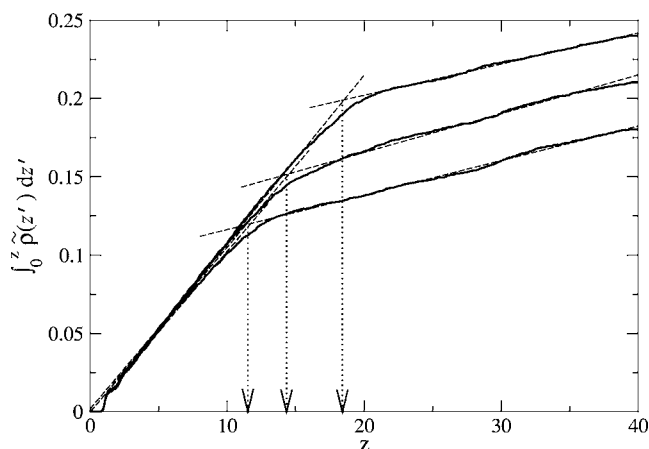
FIG. 3. Illustration of the procedure for locating the interface center, as described in the text. Shown is the running integral $\int_0^z \tilde{\rho}(\sigma, z')dz'$ for three example instantaneous density profiles that span the typical range of fluctuations. Dashed lines denote linear fits to the running integral in the pure liquid and vapor regions away from the interface. Dotted arrows show the position of the interface center determined from the intersection of the fits for each profile.

away from the interface, as illustrated in Fig. 3. We note that our centering procedure differs from that adopted in some other studies of liquid-vapor interfaces (see, e.g., [21,22]), where the origin of the interface is defined via the instantaneous Gibbs dividing surface. We consider the present method to be somewhat more straightforward to implement because use of the running integral yields a smooth function for the requisite fit in the pure phase region. By contrast, in order to locate the instantaneous Gibbs dividing surface, one must estimate the densities of the coexisting pure phases from the inherently noisy form of the instantaneous profile—a procedure which may be less reliable, particularly for systems having a small wall area. Nevertheless, we do not expect differences in the precise definition to have repercussions for the qualitative features of results. Indeed, as a check of our procedure, we have investigated the effect of disabling particle transfer MC moves (leaving operational only particle displacement and resizing moves). Doing so greatly suppresses the fluctuations in the interface thickness and yields an average profile, the shape of which agrees to within error with that obtained from the centering technique.

III. RESULTS

Before describing our findings for the liquid-vapor interfacial properties, it is instructive to quantify the nature of the fractionation in the pure phases away from the interface. This is done in Fig. 4, which displays the single liquid and vapor (daughter) phase distributions $\rho_L(\sigma)$ and $\rho_V(\sigma)$, together with the Schulz parent distribution from which they derive, all at the nominated bulk density of $n_0 = 0.089$. Clearly there is a pronounced segregation of larger particles to the liquid phase. Indeed, for $\sigma = \sigma_c = 1.6$, the density in this phase exceeds that of the vapor by a factor of two orders of magnitude far greater than the ratio of the overall number densities in the coexisting phases ($\rho_L/\rho_V \approx 5$). One notes further that,
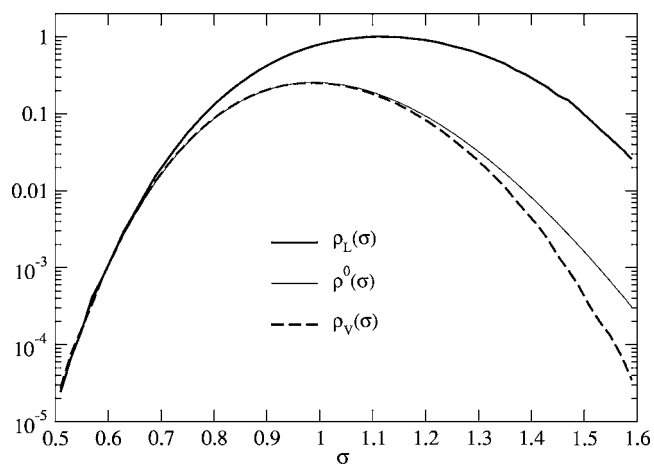

FIG. 4. Density distributions $\rho(\sigma)$ in the coexisting bulk phases at $n_0 = 0.088$, $\tilde{T} = 1.384$. Also shown is the parent form $\rho^0(\sigma)$. Statistical errors are comparable with the linewidths.

as the particle size decreases, the density distributions in both phases tend to the parent form. The origin of this feature is traceable to the fact that the smallest particles interact only very weakly [cf. Eq. (2.1)], and consequently their density is principally controlled by the imposed chemical potential, rather than the prevailing number density.

Turning now to the interfacial properties, Fig. 5 presents the measured form of the centered distribution $\rho(\sigma, z^\star)$, accumulated as described in Sec. II B. Clearly evident is the fractionation of larger particles to the liquid region. The corresponding forms of $\rho(z^\star)$ and $\eta(z^\star)$ [cf. Eqs. (2.7) and (2.9)] are given in Fig. 6(a). Also shown [Fig. 6(b)] is the variation of the average particle size $\bar{\sigma}(z^\star)$ across the interface.

We have attempted to fit $\rho(z^\star)$, $\eta(z^\star)$, and $\bar{\sigma}(z^\star)$ using a function of the standard tanh form [23,24],

$$y(z^\star|\sigma) = y_a + y_d \tanh\left[\frac{2(z_0^\star - z^\star)}{\lambda}\right], \qquad (3.1)$$

where $y_a = (y_L + y_V)/2$ and $y_d = (y_L - y_V)/2$, with y_L and y_V the appropriate limiting pure phase quantity. Here $z_0^\star$ denotes the location of the interfacial midpoint, while λ is a measure of the interfacial half-width. It should be noted that the fitting form Eq. (3.1) derives from mean-field theories of coexistence between *symmetrical* phases [23,24], and is not neces-
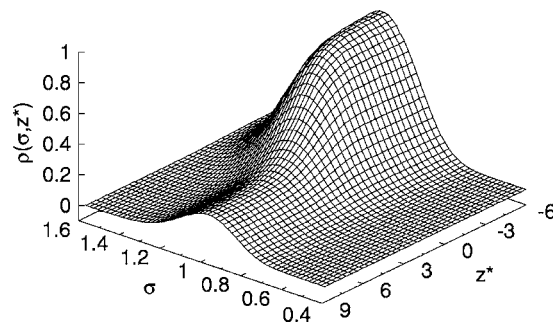

FIG. 5. The measured profile $\rho(\sigma, z^\star)$ near the liquid-gas interface, determined via the procedure de- scribed in the text.
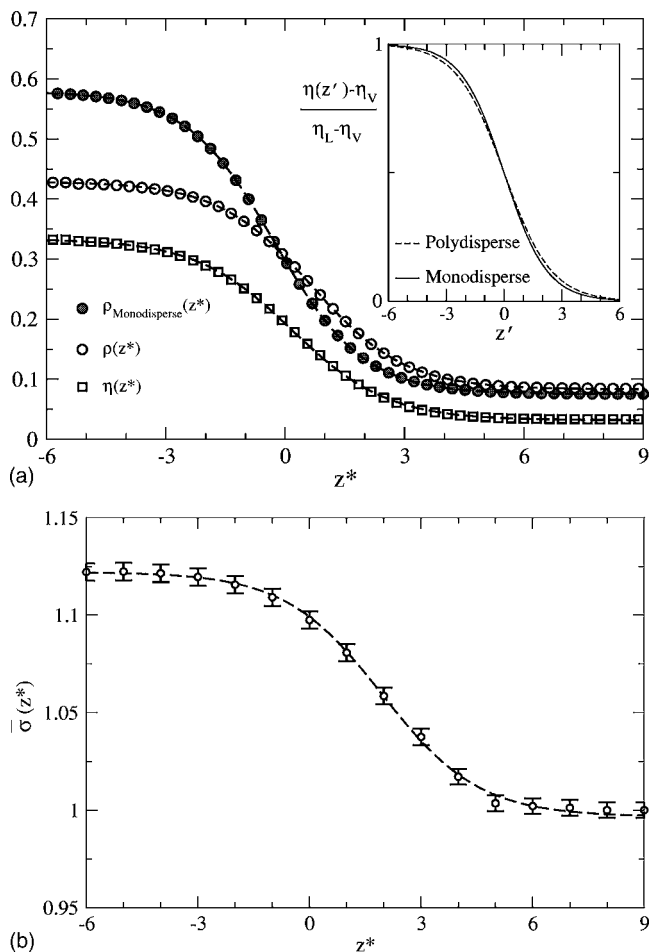
FIG. 6. (a) Estimates of the overall number density profile $\rho(z^\star)$ and volume fraction profile $\eta(z^\star)$. Lines are fits of the form Eq. (3.1). Also shown is the density profile in the monodisperse limit at $\tilde{T} = 1.080$, for which the relative volume fraction fluctuations match those of the polydisperse case (see text). The inset shows a comparison of the volume fraction profiles under these conditions. Statistical errors are smaller than the symbol sizes. (b) The variation across the interface of the average local particle size, $\bar{\sigma}(z^\star)$. The line is a fit of the form Eq. (3.1).

sarily expected to hold for real asymmetric fluids which lack particle-hole symmetry [25–27]. Nevertheless, Eq. (3.1) has been shown to provide a good description of the liquid-gas interface density profile of the monodisperse LJ fluid [28], and indeed we do appear to obtain good fits for all profiles, as evidenced in Fig. 6. The associated midpoints and interfacial widths are $z_0^\star = 0.661, w \equiv 2\lambda = 9.3(2)$ for the $\rho(z)$ profile, $z_0^\star = 0.142, w = 9.6(2)$ for $\eta(z)$, and $z_0^\star = 1.89, w = 10.4(3)$ for $\bar{\sigma}(z)$. Discrepancies in these estimates are presumably traceable to the varying sensitivity of the respective observable to the interface proximity. For example, because $\rho(z^\star)$ contains no direct information on the variation of the concentration across the interface, fits to its form possibly constitute a poorer estimator for the interfacial width than $\bar{\sigma}(z^\star)$. We shall return to this point below and in Sec. IV.

It is of interest to compare the interfacial properties of our polydisperse fluid with those of the corresponding monodisperse system. For reasons detailed in Sec. IV, we have cho-

sen to perform this comparison not at a given temperature and overall bulk number density, but under two separate conditions relating to the *volume fractions* of the coexisting pure phases. First we consider, for the monodisperse system, the temperature at which the value of the relative fluctuation $2(\eta_L - \eta_V)/(\eta_L + \eta_V)$ equals that pertaining to the polydisperse system at the state point under consideration ($\tilde{T} = 1.384, n_0 = 0.089$). This occurs for $\tilde{T} = 1.080$ [29]. The associated monodisperse density profile is included in Fig. 6(a), together with (in the inset) a comparison of the volume fraction profiles of both systems. Fitting the monodisperse volume fraction profile via the tanh form [Eq. (3.1)] yields a width estimate $w = 8.8(2)$, i.e., some 10% smaller than found for the polydisperse profile $w = 9.6(2)$. An alternative scenario compares the poly- and monodisperse systems under conditions of equal volume fraction difference $\eta_L - \eta_V$ (which occurs for the monodisperse system at $\tilde{T} = 1.048$). Under such conditions, the difference in the width estimates falls to 5%. We discuss these findings further in Sec. IV.

Given knowledge of the distribution $\rho(\sigma, z^\star)$, it is straightforward to extract the profiles for given individual species, i.e., the forms of $\rho(z^\star | \sigma)$. A representative selection of these is presented in Fig. 7, from which one observes that for smaller values of σ, a pronounced "segregation" peak occurs in the density near the interface. It is interesting to note that for the smallest particle size for which reasonable statistics could be obtained ($\sigma = 0.6$), the densities on either side of the interface barely differ, in accord with the coincidence (noted above) of the bulk daughter distributions for small σ. Notwithstanding this, a clear 10% enhancement of the density of this species occurs at the interface. That the profile $\rho(z^\star | \sigma = 0.6)$ couples to *changes* in the overall density $\rho(z^\star)$ but not its absolute value provides an indication that the segregation phenomenon is associated with the surface tension of the interface. This point is discussed further in Sec. IV.

The absolute height of the segregation peak is greatest for $\sigma \approx 0.9 - 1.0$ and is apparent in all density profiles for $\sigma \lesssim 1.0$. However, the associated segregation effect actually extends to at least $\sigma = 1.1$, as is evident from an examination of slices at a given σ through the local concentration distribution $\phi(\sigma, z^\star)$, as shown in Fig. 8. Specifically, the profile $\phi(z^\star | \sigma = 1.1)$ shows a clear peak at the interface. The fact that a peak is visible in this profile, but neither in $\rho(z^\star | \sigma = 1.1)$ nor the concentration profiles for smaller σ values, can be explained as follows. For $\sigma < 1.1$, the concentration profiles are monotonically increasing with $z^\star$ and the ratio of concentration in the vapor to that in the liquid increases rapidly with decreasing σ. For $\sigma > 1.1$, however, the profiles are monotonically decreasing and the ratio of concentration in the vapor to that in the liquid decreases rapidly with increasing σ. Accordingly, for $\sigma \approx 1.1$, the concentrations in the two phases are closely matched. This matching enhances the visibility of the segregation peak, which would otherwise be overwhelmed by the large relative variation in the concentration profile across the interface, as indeed occurs for smaller σ. This situation should be contrasted with that for $\rho(z^\star | \sigma)$, where the ratio of densities in the liquid and vapor becomes
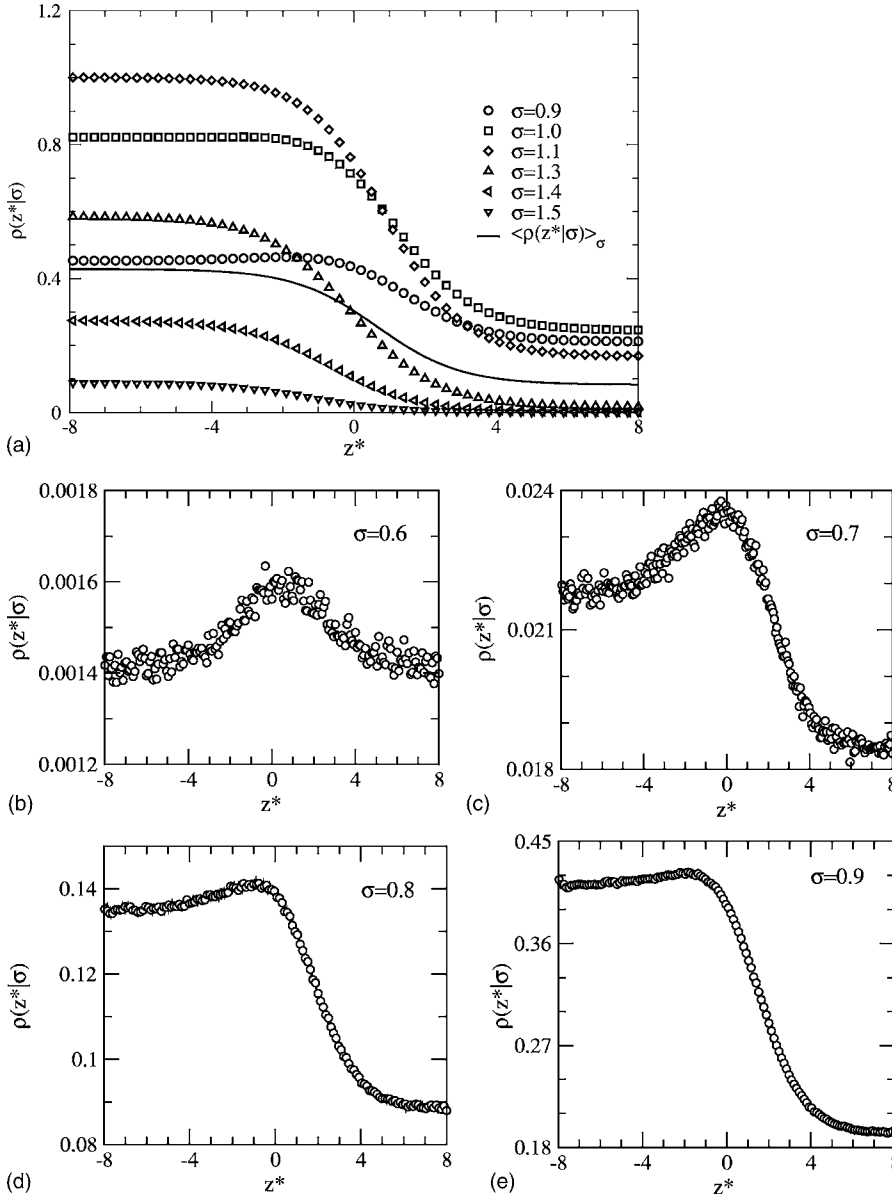
FIG. 7. (a) Estimates of interfacial density profiles $\rho(z^\star|\sigma)$ for various σ in the range $0.9 \leq \sigma \leq 1.5$. The solid line is the overall density profile $\rho(z)$. Statistical errors are smaller than the symbol sizes. (b)–(e) show the corresponding profiles for a selection of σ in the range $0.6 \leq \sigma \leq 0.9$. The statistical quality of the data becomes poor for $\sigma \lesssim 0.6$ due to the low parent density (cf. Fig. 4). Statistical errors are comparable with the spread of data points.

more closely matched as σ decreases (cf. Fig. 7), thereby enhancing the visibility of the segregation peak. Additionally, one can expect that any such peak is more distinguishable against a monotonically decreasing profile, as is the case for the density $\rho(z^\star|\sigma)$, than for monotonically increasing ones, as is the case for the concentration profiles $\phi(z^\star|\sigma)$ for $\sigma < 1.1$

A more quantitative approach to the segregation effect is provided by a quantity known as the symmetrized surface segregation, first introduced in the context of binary liquid mixtures [30,31]. This compares the interfacial density profiles of a nominated species σ with that of some reference species $\hat{\sigma}$,

$$\Delta(z^\star|\sigma,\hat{\sigma}) \equiv \frac{\rho(z^\star|\hat{\sigma}) - \rho_L(\hat{\sigma})}{a_{\hat{\sigma}\sigma}} - \frac{\rho(z^\star|\sigma) - \rho_L(\sigma)}{a_{\sigma\hat{\sigma}}}, \quad (3.2)$$

where the symmetrized concentrations are defined as

$$a_{\hat{\sigma}\sigma} = \frac{\rho_L(\hat{\sigma}) - \rho_V(\hat{\sigma})}{\rho_L(\sigma) - \rho_V(\sigma) + \rho_L(\hat{\sigma}) - \rho_V(\hat{\sigma})}, \quad (3.3)$$

$$a_{\sigma\hat{\sigma}} = \frac{\rho_L(\sigma) - \rho_V(\sigma)}{\rho_L(\sigma) - \rho_V(\sigma) + \rho_L(\hat{\sigma}) - \rho_V(\hat{\sigma})}. \quad (3.4)$$

Here $\rho_L(\sigma)$ and $\rho_V(\sigma)$ denote the density of a given species in the bulk liquid and vapor phases, respectively. $\Delta(z^\star|\sigma,\hat{\sigma})$ is, by construction, zero in the two pure phases, while at any point in the interfacial region it is either negative or positive depending on the sign of the relative segregation of the two species σ and $\hat{\sigma}$. The relative adsorption of species σ with respect to species $\hat{\sigma}$ can then be calculated as [30]

$$\Gamma(\sigma|\hat{\sigma}) = -a_{\hat{\sigma}\sigma} \int_{-\infty}^{\infty} dz^\star \Delta(z^\star|\sigma,\hat{\sigma}). \quad (3.5)$$

The density and concentration profiles discussed above show evidence of surface segregation for $\sigma \lesssim 1.1$. In seeking to
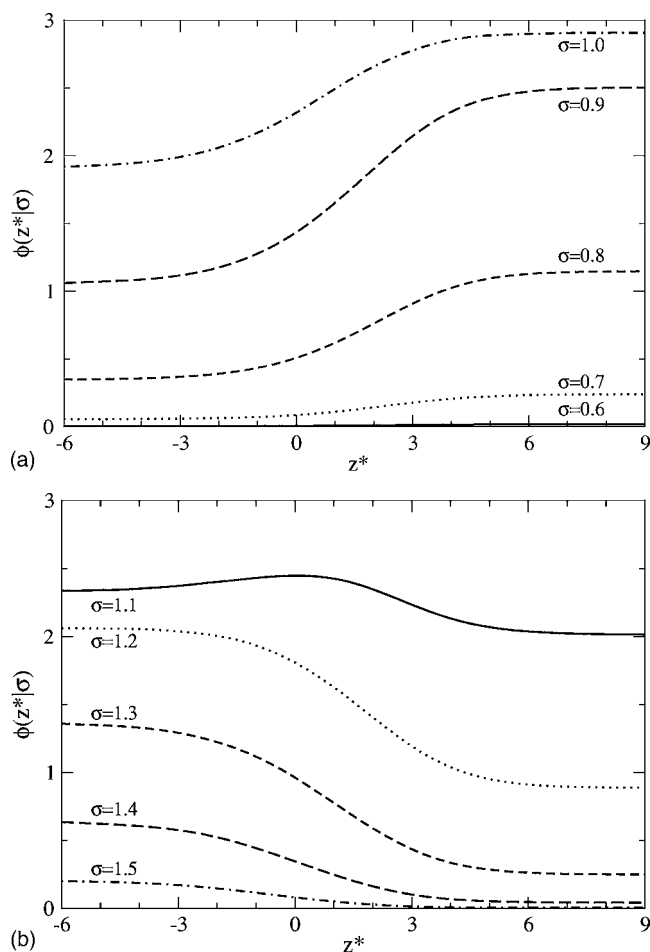
FIG. 8. A selection of profiles of the local concentration $\phi(\sigma, z^\star)$, as described in the text. Statistical errors do not exceed the linewidths.

FIG. 9. (a) Estimates of the symmetrized surface segregation $\Delta(z^\star | \sigma, \hat{\sigma})$ (see text) for a choice of the reference species $\hat{\sigma} = 1.2$. Statistical errors are comparable with the symbol size. (b) The σ-dependent adsorption relative to $\hat{\sigma} = 1.2$.

quantify surface adsorption, it therefore seems reasonable to adopt as the reference species $\hat{\sigma} = 1.2$, for which no segregation was discernible [33]. The corresponding forms of $\Delta(z^\star | \sigma, \hat{\sigma})$ are shown in Fig. 9(a), together with the relative adsorption $\Gamma(\sigma | \hat{\sigma})$ in Fig. 9(b). The latter figure clearly shows the adsorption peaking at around $\sigma = 0.9 - 1.0$. The population of particles having size $\sigma > 1.2$ are depleted in comparison. We note that the adsorption can be readily calculated via alternative approaches, such as that based on the construction of a Gibbs dividing surface for the reference species [15,32]. As a check on our procedure, we have also applied this approach, finding results that are numerically practically indistinguishable from those obtained from Eq. (3.5).

In a previous study of the liquid-vapor interface of a binary fluid mixture [31], the forms of $\Delta(z^\star)$ were argued to provide a more reliable measure of the interfacial width than that provided by tanh fits to the overall density profile $\rho(z^\star)$ alone, which tend to underestimate the true width. Adopting the criterion [31] that the width is given by the range of $z^\star$ for which $|\Delta(z^\star)|$ exceeds 5% of its maximum value, knowledge of $\Delta(z^\star | \sigma, \tilde{\sigma})$ provides estimates of the interfacial width $w(\sigma)$ for each σ. This quantity exhibits a spread of values, the largest corresponding to the largest species,
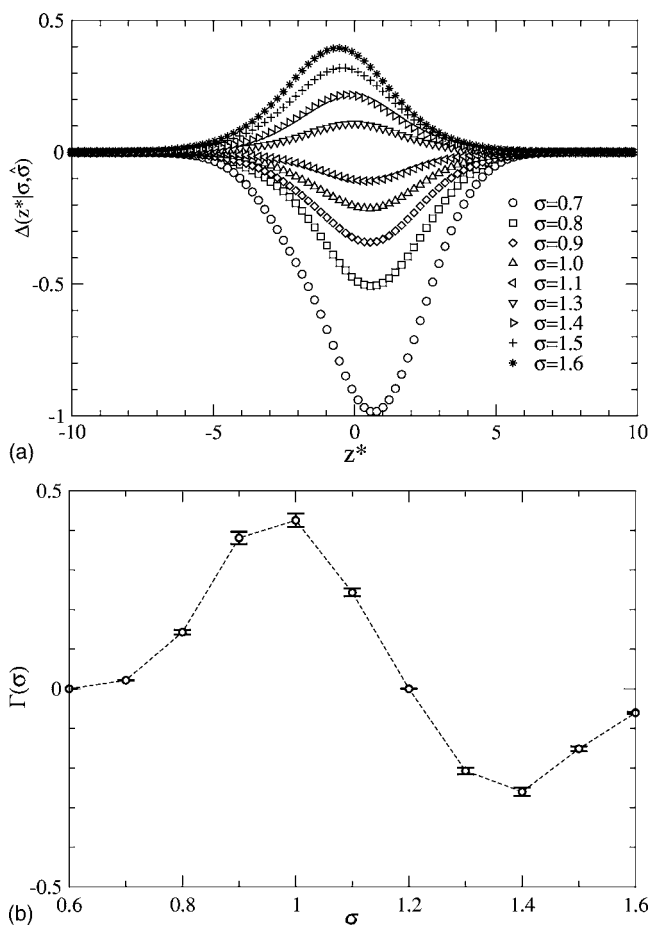
$w(\sigma = 1.6) = 10.4(3)$, a value which indeed clearly exceeds that of $w = 9.3(2)$ arising from the tanh fit to the density profile $\rho(z^\star)$. It is, however, somewhat closer to that obtained from the fit to $\eta(z^\star)$ [i.e., $w = 9.6(2)$], and agrees well with the estimate $w = 10.4(2)$ obtained for the fit to $\bar{\sigma}(z^\star)$. We postpone further discussion of this comparison until Sec. IV.

Having examined the density and concentration profiles and associated adsorption, we turn finally to consider the variation of the normalized size distribution $f(\sigma)$ across the interface, Eq. (2.11). The forms of $f(\sigma | z^\star)$ for selected values of $z^\star$ spanning the interface are shown in Fig. 10(a). From the figure, one observes that on traversing from the pure liquid to the pure vapor, the size distribution steadily narrows, while its mean shifts to lower σ [cf. Figs. 4 and 6(b)]. The scale of the evolution of the fractionation across the interface becomes more apparent when referenced with respect to one of the pure phases (we have chosen the vapor) and plotted on a log scale, as shown in Fig. 10(b).

IV. DISCUSSION AND CONCLUSIONS

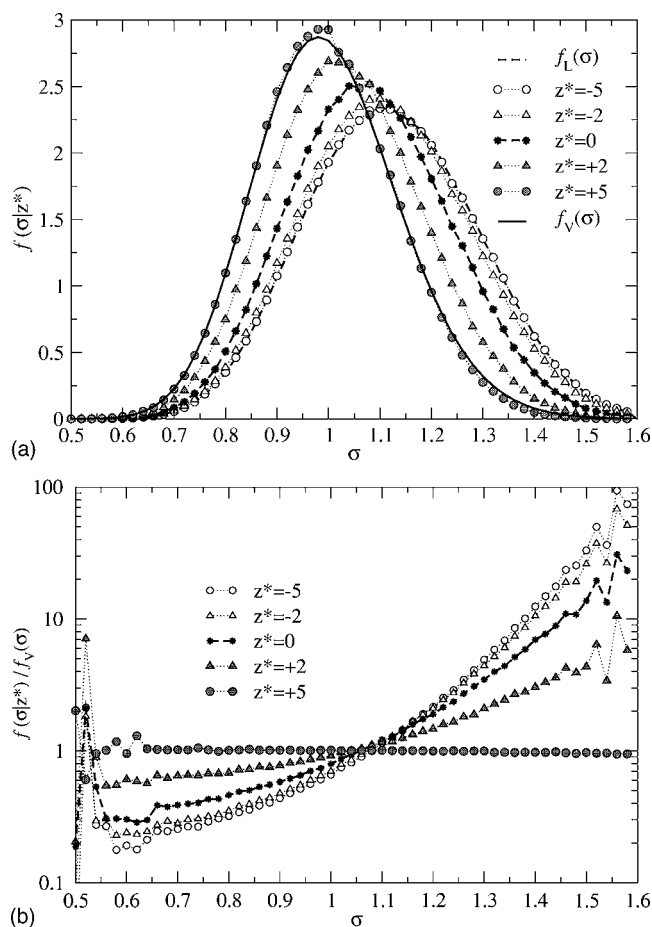In summary, we have performed a detailed simulation study of the liquid-vapor interface of a polydisperse fluid.

FIG. 10. (a) Variation of the normalized local size distribution $f(\sigma|z^\star)$ across the interface, as described in the text. Lines through symbols are merely guides to the eye. (b) The same data referenced with respect to the vapor phase distribution, and expressed on a log scale.

The main feature of our results is the finding of a preferential adsorption of smaller particles at the interface and a corresponding depletion of larger ones. This confirms the predictions of density-functional theory for a polydisperse van der Waals fluid [15]. We note, however, that the segregation phenomenon is not peculiar to the case of polydisperse mixtures. Analogous effects are well known to occur in the context of binary fluid mixtures, where one component is often preferentially absorbed at the liquid-gas boundary (see, e.g., Refs. [22,30,34–37]). The segregation occurs because coating the interface in the more volatile (less strongly interacting) of the two species reduces the surface tension, as can be shown from the Gibbs adsorption equation [32]. In view of this, one might expect that for the polydisperse system, the smallest species should be maximally adsorbed. In contrast, we find that the adsorption is actually greatest for an intermediate size (cf. Fig. 9). This finding can be understood from the fact that for our interparticle potential [Eq. (2.1)], the smallest particles interact only weakly with one another (and indeed become ideal in the limit $\sigma \rightarrow 0$). Coating the interface in such very small particles cannot, therefore, screen the larger ones and reduce the surface tension.

We have examined various quantities which provide measures of the liquid-vapor interfacial width. Good fits of the

tanh form [Eq.(3.1)] were achieved for the profiles of the overall number density, volume fraction, and local average particle size. Additionally, a further measure, the 95% width of the symmetrized surface segregation profile, $\Delta(z^\star|\sigma,\tilde{\sigma})$, was examined [31]. This latter quantity contains explicit information on the density profiles of the individual species $\rho(z^\star|\sigma)$, which, it seems, is important in obtaining reliable estimates of the interfacial width. By contrast, the overall profiles $\rho(z^\star)$ and $\eta(z^\star)$, integrate out some, or all, of the σ dependence of $\rho(\sigma,z^\star)$. They thus suppress information about species whose individual profile width is large, but which contribute relatively little weight to the overall density. This may result in an underestimate of the true length scale over which the system properties deviate from their bulk values, and indeed the discrepancies we find in the interfacial width for the various profiles (Sec. III) provide some evidence for this. We note further that if one simply examines the overall density profile, one may miss important features such as the segregation peak, which is apparent in $\rho(z^\star|\sigma)$ for small σ, but not in $\rho(z^\star)$.

Turning now to the effects of polydispersity on the width of the liquid-vapor interface, it is stated in Ref. [15] that polydispersity broadens the interface compared to the monodisperse limit. However, our results highlight the need for care when attempting to isolate the intrinsic effects of polydispersity on the interfacial width from those arising indirectly as a result of polydispersity-induced alterations to the bulk phase behavior. Indeed, the latter may well constitute the dominant factor. For example, introducing polydispersity of the form described by Eq. (2.1) (which is similar to that considered in [15]) tends to raise the critical temperature sharply with respect to the monodisperse limit [8,17]. Thus on increasing the degree of polydispersity at a *given* temperature, one can expect the interface to become sharper since the system moves deeper into the two-phase region. Our results provide an extreme example of this. Specifically, the temperature at which we studied phase coexistence in the polydisperse system, $\tilde{T}=1.384$, exceeds the corresponding critical temperature in the monodisperse limit, namely $\tilde{T}_c =1.1876$ [29]. Thus at $\tilde{T}=1.384$ no interface would occur at all in the monodisperse limit.

Another issue which complicates comparison of interfacial widths in polydisperse and monodisperse systems is the choice of parent density n_0. Owing to fractionation and the resulting smearing of the phase diagram (cf. Fig. 1), the value of n_0 constitutes a crucial factor in determining the properties of the coexisting bulk phases and thence the interface between them. Again the present work provides a case in point: although we studied the system at the critical temperature, true phase coexistence was nevertheless observable because n_0 was less than the critical value. Indeed, one can obtain a sharper or a broader interface simply by changing n_0 at constant T, a situation which contrasts with that in the monodisperse limit.

Thus we believe that when trying to isolate the intrinsic contribution of polydispersity to interfacial widths, one should endeavor to perform the comparison at points in the phase diagram that are, in the sense of corresponding states theory, equivalent in terms of their relative deviation from

criticality. Matching the bulk volume fraction fluctuations (in preference to the densities which do not provide equivalent information) seems one reasonable way to do this. Doing so [cf. inset of Fig. 6(a)] shows that polydispersity may only broaden the interface marginally (5–10 %). We caution, however, that our study is far from comprehensive in this regard. Indeed, owing to the currently high computational investment required to study polydisperse systems, we were only able to investigate the interfacial properties for a single parent form at a single coexistence state point. It is possible that interfacial segregation and its effect on the surface tension and interfacial width might become more significant at state points further removed from criticality [15] and for other forms of the parent distribution. Measurements of the surface tension for a range of different parent forms and state points would doubtlessly throw more light on the segregation phenomena. For the time being, however, the computational cost of such a study remains prohibitive.

ACKNOWLEDGMENTS

[1] J. J. Salacuse and G. Stell, J. Chem. Phys. **77**, 3714 (1982).

[2] R. G. Larson, *The Structure and Rheology of Complex Fluids* (Oxford University Press, New York, 1999).

[3] P. Chaikin, in *Soft and Fragile Matter*, edited by M. E. Cates and M. R. Evans (IOP Publishing, London, 2000).

[4] S. Chandrasekhar, *Liquid Crystals* (Cambridge University Press, Cambridge, 1992).

[5] H.-G. Elias, *An Introduction to Polymer Science* (Wiley-VCH Publishers, Weinheim, 1997).

[6] P. Sollich, J. Phys.: Condens. Matter **14**, R79 (2002).

[7] C. Rascón and M. E. Cates, J. Chem. Phys. **118**, 4312 (2003).

[8] L. Bellier-Castella, H. Xu, and M. Baus, J. Chem. Phys. **113**, 8337 (2000).

[9] P. Bryk, A. Patrykiejew, J. Reszko-Zygmunt, S. Sokolowski, and D. Henderson, J. Chem. Phys. **111**, 6047 (1999).

[10] I. Pagonabarraga, M. E. Cates, and G. J. Ackland, Phys. Rev. Lett. **84**, 911 (2000).

[11] M. Buzzacchi, I. Pagonabarraga, and N. B. Wilding, J. Chem. Phys. **121**, 11362 (2004).

[12] R. P. A. Dullens and W. K. Kegel, Phys. Rev. Lett. **92**, 195702 (2004).

[13] O. Pizio, A. Patrykiejew, and S. Sokolowski, Mol. Phys. **99**, 57 (2001).

[14] S.-C. Kim, J. Chem. Phys. **114**, 9593 (2001).

[15] L. Bellier-Castella, H. Xu, and M. Baus, Phys. Rev. E **65**, 021503 (2002); M. Baus, L. Bellier-Castella, and H. Xu, J. Phys.: Condens. Matter **14**, 9255 (2002).

[16] N. B. Wilding and P. Sollich, J. Chem. Phys. **116**, 7716 (2002).

[17] N. B. Wilding, M. Fasolo, and P. Sollich (unpublished).

[18] N. B. Wilding, J. Chem. Phys. **119**, 12163 (2003).

[19] N. B. Wilding and P. Sollich, Europhys. Lett. **67**, 219 (2004).

[20] N. B. Wilding, M. Fasolo, and P. Sollich, J. Chem. Phys. **121**, 6887 (2004).

[21] J. Fischer and M. Methfessel, Phys. Rev. A **22**, 2836 (1980).

[22] J. Alejandre, Y. Duda, and S. Sokolowski, J. Chem. Phys. **118**, 329 (2003).

[23] J. W. Cahn and J. E. Hilliard, J. Chem. Phys. **28**, 258 (1958); **31**, 688 (1959).

[24] S. Fisk and B. Widom, J. Chem. Phys. **50**, 3219 (1969).

[25] P. G. de Gennes, J. Phys. (Paris), Lett. **42**, L377 (1981).

[26] J. A. Barker and J. R. Henderson, J. Chem. Phys. **76**, 6303 (1982).

[27] I. Szleifer, J. Chem. Phys. **92**, 6940 (1990).

[28] C. D. Holcomb, P. Clancy, and J. A. Zollweg, Mol. Phys. **78**, 437 (1993).

[29] N. B. Wilding, Phys. Rev. E **52**, 602 (1995).

[30] M. M. Telo da Gama and R. Evans, Mol. Phys. **48**, 251 (1983).

[31] J. Winkelmann, J. Phys.: Condens. Matter **13**, 4739 (2001).

[32] J. S. Rowlinson and B. Widom, *Molecular Theory of Capilliarity* (Clarendon, Oxford, 1982).

[33] An alternative approach is to calculate the adsorption taking the reference to be the overall density profile $\rho(z)$, rather than the density profile for $\sigma=1.2$. Doing so leaves the qualitative features of our results unchanged.

[34] G. A. Chapela, G. Saville, S. M. Thompson, and J. S. Rowlinson, J. Chem. Soc., Faraday Trans. 2, **73**, 1133 (1977).

[35] P. Smith, R. M. Lynden-Bell, and W. Smith, Mol. Phys. **98**, 255 (2000).

[36] W. Prange, T. Kurbjuhn, M. Tolan, and W. Press, J. Phys.: Condens. Matter **13**, 4957 (2001).

[37] S. Latsevich and F. Forstmann. J. Chem. Phys. **107**, 6925 (1997).